# Current-induced spin polarization in a two-dimensional hole gas

Chao-Xing Liu,[1,2] Bin Zhou,[2] Shun-Qing Shen,[2] and Bang-fen Zhu[1]
[1]*Department of Physics and Center for Advanced Study, Tsinghua University, Beijing 100084, China*
[2]*Department of Physics and Center of Computational and Theoretical Physics, The University of Hong Kong, Hong Kong, China*
(Received 21 December 2007; revised manuscript received 21 February 2008; published 31 March 2008)

We investigate the current-induced spin polarization in the two-dimensional hole gas (2DHG) with the structure inversion asymmetry. By using the perturbation theory, we rederive the effective *k*-cubic Rashba Hamiltonian for 2DHG and the generalized spin operators accordingly. Then based on the linear response theory, we analytically and numerically calculate the current-induced spin polarization with the disorder effect considered. We have found that, quite different from the two-dimensional electron gas, the spin polarization in 2DHG linearly depends on Fermi energy in the low-doping regime, and with increasing Fermi energy, the spin polarization may be suppressed and even changes its sign. We predict a pronounced peak of the spin polarization in 2DHG once the Fermi level is somewhere between the minimum points of two spin-split branches of the lowest light-hole subband. We discuss the possibility of measurements in experiments as regards the temperature and the width of quantum wells.

DOI: 10.1103/PhysRevB.77.125345 PACS number(s): 72.25.−b, 85.75.−d, 71.70.Ej, 72.25.Pn

## I. INTRODUCTION

In order to reduce the electric leakage and to meet the challenge brought about by the reduced physical size of the future nanoelectronics, the replacement of the electron charge with the spin degree of freedom in the electronic transport is being explored. This is the ambitious goal of researchers in the field of spintronics.[1–3] One of the basic issues in this field is how to generate the polarized spin in devices. In a straightforward way, the spin injection from ferromagnetic layers may provide a possible solution to this problem if the interface mismatch problem can be avoided, but it is more desirable to directly generate spin polarization by electric means in devices because of its easy controllability and compatibility with the standard microelectronics technology.[1–3] The spin-orbit coupling (SOC) in semiconductors, which relates the electron spin to its momentum, may provide a controllable way to realize such a purpose. Based on this idea, the phenomenon of current-induced spin polarization (CISP) has recently attracted extensive attention of a lot of research groups.[4–26]

As early as the 1970s, the CISP due to the spin-orbit scattering near the surface of semiconductor thin films was predicted by Dyakonov and Perel.[4] Restricted by experimental conditions at that time, this prediction was ignored until the beginning of the 1990s. With the development of sample fabrication and characterization technology in low-dimensional semiconductor systems, it was realized that such phenomena could also exist in quantum wells and heterostructures with the structure or bulk inversion asymmetry.[5,6] Later, many interesting topics about CISP have been raised, such as the joint effect of the Rashba and Dresselhaus SOC mechanism,[7] vertex correction,[5–8] quantum correction,[9,10] and resonant spin polarization.[11] Experimentally, CISP was first observed by Silov *et al.*[12] in a two-dimensional hole gas (2DHG) by using the polarized photoluminescence.[27–29] When inputting an in-plane current into the 2DHG system, they observed a large optical polarization in photoluminescence spectra.[12] Later, Kato *et al.*[13,14] demonstrated the existence of the CISP in strained nonmagnetic semiconductors, and Sih *et al.*[15] detected the CISP in the two-dimensional electron gas (2DEG) in (110) AlGaAs quantum well.[15] The CISP was also found in ZnSe epilayers even up to room temperature.[16] Very recently, the converse effect of CISP has been clearly shown by Yang *et al.*[17] experimentally, and the spin photocurrent has also been observed.[18–20]

So far, most theoretic investigations about the CISP deal with the electron SOC systems.[4–10,21–26,30–32] Thus, the CISP in the 2DHG system as shown in the experiments of Silov *et al.*[12] was also interpreted in terms of the linear-*k* Rashba coupling of the 2DEG systems with several parameters adjusted. As we shall show later, this treatment is not appropriate for 2DHG. Unlike the electron system, the hole state in the Luttinger–Kohn Hamiltonian[33] is a spinor of four components. As each component is a combination of spin and orbit momentum, the spin of a hole spinor is not a conserved physical quantity. Therefore, the "spintronics" for hole gas is, in fact, a combination of spintronics and orbitronics.[34,35] If only the lowest heavy-hole (HH1) subband is concerned, by projecting the multiband Hamiltonian of 2DHG with structural inversion asymmetry into a subspace spanned by $|\pm\frac{3}{2}\rangle$ mostly relevant with the HH1 states, we can obtain the *k*-cubic Rashba model.[36–41] Here, we emphasize in this lowest heavy-hole subspace that the spin operators are no longer represented by three Pauli matrices, because the "generalized spin" we shall adopt is a hybridization of spin and orbit angular momentum.[34] In deriving the effective Hamiltonian from the Luttinger–Kohn Hamiltonian by the perturbation and truncation procedure to higher orders, one must take care of the corresponding transformation for the spin operator in order to obtain the correct expression. In the following, we will use the terminology generalized spin, or the "spin" for short, to denote the total angular momentum in the spin-orbit coupled systems.

The aim of the present paper is to investigate the CISP of a 2DHG in a more rigorous way. Namely, we will derive the *k*-cubic Rashba model and the corresponding spin operators for holes, and on this basis, we will present both analytical

 

and numerical results for the CISP in a 2DHG. This paper is organized as follows. In Sec. II, the general formalism and the Hamiltonian for the 2DHG with structural inversion asymmetry are given. In Sec. III, in the low-doping regime, with the perturbation theory, the Hamiltonian and spin operators in the lowest heavy-hole subspace are derived and applied to the analytical calculation of the CISP in a 2DHG. In Sec. IV, we will show that the numerical calculations agree well with the analytical results at the low-doping regime, while in the high-doping regime, the numerical results predict some additional features of CISP. Particularly, we predict a pronounced CISP peak when the Fermi energy lies a little above the energy minimum of the lowest light-hole (LH1) subband. Finally, a brief summary is drawn.

## II. FORMALISM

### A. Hole Hamiltonian

A $p$-doped quantum well system with structural inversion asymmetry can be described as the isotropic Luttinger–Kohn Hamiltonian with a confining asymmetrical potential,

$$\hat{H} = \hat{H}_L + \hat{V}_c(z) + \hat{V}_a(z). \tag{1}$$

Here, in order to compare the analytical results with the numerical one, the confining potential along the $z$ direction $V_c(z)$ is taken as

$$\hat{V}_c(z) = \begin{cases} 0, & -L_z/2 < z < L_z/2 \\ \infty & \text{otherwise}, \end{cases} \tag{2}$$

where $L_z$ is the well width of the quantum well. The asymmetrical potential, which stems from a built-in electric field $F$ via the gate voltage or $\delta$ doping, is $\hat{V}_a(z)=eFz$, which breaks the inversion symmetry and lifts the spin doublet degeneracy.

Let $\hat{S}$ be the generalized spin operator of a hole state, and $\hat{S}_z$ be the $z$ component of $\hat{S}$, the isotropic Luttinger–Kohn Hamiltonian $\hat{H}_L$ in the $|S,S_z\rangle$ representation (four basis kets written in the sequence of $\{|\frac{3}{2}\rangle,|\frac{1}{2}\rangle,-\frac{1}{2}\rangle,|-\frac{3}{2}\rangle\}$) is expressed as

$$\hat{H}_L = \begin{pmatrix} P & R & T & 0 \\ R^\dagger & Q & 0 & T \\ T^\dagger & 0 & Q & -R \\ 0 & T^\dagger & -R^\dagger & P \end{pmatrix}, \tag{3}$$

with

$$P = \frac{\hbar^2}{2m_0}[(\gamma_1+\gamma_2)\mathbf{k}^2 + (\gamma_1-2\gamma_2)k_z^2], \tag{4}$$

$$Q = \frac{\hbar^2}{2m_0}[(\gamma_1-\gamma_2)\mathbf{k}^2 + (\gamma_1+2\gamma_2)k_z^2], \tag{5}$$

$$R = -\frac{\hbar^2\sqrt{3}\gamma_2}{m_0}\mathbf{k}_- k_z, \tag{6}$$

$$T = -\frac{\hbar^2\sqrt{3}\gamma_2}{2m_0}\mathbf{k}_-^2, \tag{7}$$

where $\gamma_1, \gamma_2$ are the Luttinger parameters, $m_0$ is the free electron mass, the in-plane wave vector $\mathbf{k}=(k_x,k_y)$, denoted in the polar coordinate as $\mathbf{k}\equiv(k,\theta)$, $\mathbf{k}_\pm \equiv k_x \pm ik_y$, and $k_z = -i\partial/\partial z$. The other terms, such as the anisotropic term, $C$ terms, or hole Rashba term,[40–42] have only negligible effects and are omitted in our calculation. Correspondingly, the $x$, $y$, and $z$ components of the spin $-\frac{3}{2}$ operator respectively reads[43,44]

$$\hat{S}_x = \frac{1}{2}\begin{pmatrix} 0 & \sqrt{3} & 0 & 0 \\ \sqrt{3} & 0 & 2 & 0 \\ 0 & 2 & 0 & \sqrt{3} \\ 0 & 0 & \sqrt{3} & 0 \end{pmatrix}, \tag{8}$$

$$\hat{S}_y = \frac{i}{2}\begin{pmatrix} 0 & -\sqrt{3} & 0 & 0 \\ \sqrt{3} & 0 & -2 & 0 \\ 0 & 2 & 0 & -\sqrt{3} \\ 0 & 0 & \sqrt{3} & 0 \end{pmatrix}, \tag{9}$$

$$\hat{S}_z = \frac{1}{2}\begin{pmatrix} 3 & 0 & 0 & 0 \\ 0 & 1 & 0 & 0 \\ 0 & 0 & -1 & 0 \\ 0 & 0 & 0 & -3 \end{pmatrix}. \tag{10}$$

Here, we stress again that the spin of the $\frac{3}{2}$ spinor is actually its total angular momentum, which is a linear combination of spin and orbit angular momentum of a valence band electron. In polarized optical experiments, such as polarized photoluminescence[27–29] or Kerr–Faraday rotation,[13,14] it is appropriate to introduce such a generalized spin.

For the infinitely confining potential, we expand the eigenfunction $\phi_\nu$ associated with the $\nu$th hole subband in terms of confined standing waves as

$$\phi_\nu(\mathbf{k}) = \sum_{n,\lambda_h} a^\nu_{n,\lambda_h}(\mathbf{k})\frac{1}{2\pi}e^{i\mathbf{k}\cdot\mathbf{r}}|n,\lambda_h\rangle_h, \tag{11}$$

with

$$|n,\lambda_h\rangle = \sqrt{\frac{2}{L_z}}\sin\left(\frac{n\pi(z+L_z/2)}{L_z}\right)|\lambda_h\rangle, \tag{12}$$

where $\mathbf{r}=(x,y)$, $n$ is the confinement quantum number for the standing wave along the $z$ direction, and $\lambda_h$ denotes the $\lambda_h$ component of the hole ($\lambda_h=3/2,1/2,-1/2,-3/2$). Since we are only interested in the low energy physics, a finite number of $n$ will result in a reasonable accuracy and the effective Hamiltonian is reduced into a square matrix with a dimension of $4n$. In this way, we analytically or numerically obtain the hole subband structure.

### B. Expression for current-induced spin polarization

In the framework of the linear response theory, the electric response of spin polarization in a weak external electric field **E** can be formulated as[11]

$$\langle \hat{S}_\alpha \rangle = \sum_\beta \chi_{\alpha\beta} E_\beta, \tag{13}$$

where $\langle \hat{S}_\alpha \rangle$ is the thermodynamically averaged value of the spin density. The electric spin susceptibility $\chi_{\alpha\beta}$ can be calculated by the Kubo formula.[45] By the Green function formalism, the Bastin version of the Kubo formula[46] reads

$$\chi_{\alpha\beta} = \frac{ie\hbar}{2\pi} \int dE f(E) \mathrm{Tr} \left\langle \hat{S}_\alpha \left( \frac{dG^R}{dE} v_\beta A - A v_\beta \frac{dG^A}{dE} \right) \right\rangle_c, \tag{14}$$

where $G^R$ and $G^A$ are the retarded and advanced Green function, respectively, $A = i(G^R - G^A)$ is the spectral function, $f(E)$ is the Fermi distribution function, $v_\beta$ is the velocity operator along the $\beta$ direction, and the bracket $\langle \cdots \rangle_c$ represents the average over the impurity configuration.

To take the vertex correction into account, we use the Streda–Smrcka division of the Kubo formula,[46,47]

$$\chi_{\alpha\beta} = -\frac{e\hbar}{2\pi} \int dE \frac{\partial f(E)}{\partial E} \mathrm{Tr} \langle \hat{S}_\alpha G^R(E_F) v_\beta G^A(E_F) \rangle_c, \tag{15}$$

in which we retain only the nonanalytical part and neglect the analytical part, because the latter is much less important in the present case. In the following, we will use Eq. (15) to analytically calculate the electric spin susceptibility (ESS) with the vertex correction considered; meanwhile, we will carry out the numerical calculation with Eq. (14) in the first-order Born approximation. We shall show that the analytical and numerical results are in good agreement with each other in the regime of low hole density.

### C. Symmetry

The general properties of $\chi_{\alpha\beta}$ will be critically determined by the symmetry of the system. For the two-dimensional system we investigate, the index $\alpha(\beta)$ in Eq. (13) is simply chosen to be $x$ or $y$ in the following. Without the asymmetrical potential $V_a$, the Hamiltonian (1) is invariant under the space inversion transformation

$$x \to -x, \quad y \to -y, \quad z \to -z,$$

$$\hat{S}_x \to \hat{S}_x, \quad \hat{S}_y \to \hat{S}_y, \quad \hat{S}_z \to \hat{S}_z, \tag{16}$$

if the point of origin of the $z$ axis is set at the midplane of the quantum well. By applying the space inversion transformation (16) to Eq. (13), we have

$$\langle \hat{S}_\alpha \rangle = \chi_{\alpha\beta} E_\beta \to \langle \hat{S}_\alpha \rangle = -\chi_{\alpha\beta} E_\beta, \tag{17}$$

whereby $\chi_{\alpha\beta} = -\chi_{\alpha\beta}$. This implies that no CISP appears when the inversion symmetry exists in the system. So the asymmetrical potential $V_a$ is crucial for the CISP.

In the presence of an asymmetrical potential $V_a$, the Hamiltonian (1) is invariant versus the rotation along the $z$ axis with $\frac{\pi}{2}$ in both the real space and the spin space,

$$x \to y, \quad y \to -x, \quad z \to z,$$

$$\hat{S}_x \to \hat{S}_y, \quad \hat{S}_y \to -\hat{S}_x, \quad \hat{S}_z \to \hat{S}_z. \tag{18}$$

With the above transformations (18), Eq. (13) will give

$$\langle \hat{S}_x \rangle = \chi_{xy} E_y \to \langle \hat{S}_y \rangle = -\chi_{xy} E_x, \tag{19}$$

$$\langle \hat{S}_x \rangle = \chi_{xx} E_x \to \langle \hat{S}_y \rangle = \chi_{xx} E_y. \tag{20}$$

By combining with $\langle \hat{S}_y \rangle = \chi_{yx} E_x$ and $\langle \hat{S}_y \rangle = \chi_{yy} E_y$, we get

$$\chi_{xy} = -\chi_{yx}, \tag{21}$$

$$\chi_{xx} = \chi_{yy}, \tag{22}$$

which are a direct consequence of the rotation symmetry along the $z$ axis.

## III. ANALYTICAL RESULTS FOR CURRENT-INDUCED SPIN POLARIZATION IN A TWO-DIMENSIONAL HOLE GAS

In the low hole density regime, an effective Hamiltonian can be obtained by projecting the Hamiltonian (1) into the subspace spanned by the lowest heavy-hole states, which, by using the truncation approximation and projection perturbation method,[40–42,48–52] is reduced to the widely used $k$-cubic Rashba model. More importantly, the corresponding spin operators in the subspace will be obtained properly and the ESS of 2DHG with the impurity vertex correction will be worked out. Then we will compare and contrast the different behaviors of the CISP in the 2DEG and 2DHG in this section.

### A. $k$-cubic Rashba model

To obtain an approximate analytical expression, we take the following procedure. First, we expand a hole state in terms of eight basis wave functions associated with $|n, \lambda_h\rangle$ ($n = 1, 2$ and $\lambda_h = \frac{3}{2}, \frac{1}{2}, -\frac{1}{2}, -\frac{3}{2}$) [Eq. (12)]. Then for a given **k**, we may express the Hamiltonian (1) in terms of an $8 \times 8$ matrix, which by the perturbation procedure can be further projected into the subspace spanned by the $|1, \frac{3}{2}\rangle$ and $|1, -\frac{3}{2}\rangle$ states. Thus, we obtain the following $2 \times 2$ matrix (see Appendix A for details):

$$\hat{H}_{k^3} = \frac{\hbar^2 k^2}{2m_h} + i\alpha(k_-^3 \sigma_+ - k_+^3 \sigma_-), \tag{23}$$

where the Pauli matrix $\sigma_\pm \equiv \frac{1}{2}(\sigma_x \pm i\sigma_y)$, the effective mass is renormalized to

$$m_h = m_0 \left( \gamma_1 + \gamma_2 - \frac{256\gamma_2^2}{3\pi^2(3\gamma_1 + 10\gamma_2)} \right)^{-1}, \tag{24}$$

and the $k$-cubic Rashba coefficient

$$\alpha = \frac{512 e F L_z^4 \gamma_2^2}{9\pi^6 (3\gamma_1 + 10\gamma_2)(\gamma_1 - 2\gamma_2)}. \tag{25}$$

Note that Eq. (23) is just the $k$-cubic Rashba model, in which the Rashba coefficient $\alpha$ is proportional to the asymmetrical

potential strength $F$, in agreement with the results by Winkler.[40] We can rewrite the $k$-cubic Rashba Hamiltonian (23) as

$$\hat{H}_{k^3} = \varepsilon(\mathbf{k}) + \sum_{i=x,y,z} d_i(\mathbf{k})\sigma_i, \tag{26}$$

where $d_x = \alpha k_y(3k_x^2 - k_y^2)$, $d_y = \alpha k_x(3k_y^2 - k_x^2)$, $d_z = 0$, and $\varepsilon(\mathbf{k}) = \frac{\hbar^2 k^2}{2m_h}$. The eigenvalue associated with the spin index $\mu$ ($\mu = \pm 1$) is

$$E_\mu(k) = \varepsilon(\mathbf{k}) + \mu\alpha k^3, \tag{27}$$

with the eigenfunction

$$\psi_{\mathbf{k}\mu}(\mathbf{r}) = \frac{e^{i\mathbf{k}\cdot\mathbf{r}}}{\sqrt{2A_S}}\begin{pmatrix} i \\ \mu e^{i3\theta} \end{pmatrix}, \tag{28}$$

where $A_S$ is the area of the system.

The $k$-cubic Rashba model has been widely used to study the spin Hall effect in 2DHG;[36–38,53] however, insufficient attention has been given to the corresponding spin operators. For example, although Hamiltonian (23) is written in terms of the Pauli matrices $\sigma$, the $\sigma$ matrix is no longer directly related to the spin. The correct spin operators in the $k$-cubic Rashba model, as described in Appendix A, are expressed as

$$\tilde{S}_x = \begin{pmatrix} -S_0 k_y & S_1 k_-^2 \\ S_1 k_+^2 & -S_0 k_y \end{pmatrix}, \tag{29}$$

$$\tilde{S}_y = \begin{pmatrix} S_0 k_x & -iS_1 k_-^2 \\ iS_1 k_+^2 & S_0 k_x \end{pmatrix}, \tag{30}$$

$$\tilde{S}_z = \frac{3}{2}\sigma_z, \tag{31}$$

in which

$$S_0 = \frac{512\gamma_2 L_z^4 eFm_0}{9\pi^6\hbar^2(3\gamma_1 + 10\gamma_2)(\gamma_1 - 2\gamma_2)}, \tag{32}$$

$$S_1 = \left[\frac{3}{4\pi^2} - \frac{256\gamma_2^2}{3\pi^4(3\gamma_1 + 10\gamma_2)^2}\right]L_z^2. \tag{33}$$

Clearly, the coefficient $S_0$ and the Rashba coefficient $\alpha$ have the same dependence on $F$ and $L_z$, thus we have

$$S_0 = \frac{\alpha m_0}{\hbar^2\gamma_2}. \tag{34}$$

$S_z$ is related to $\sigma_z$, while $S_x(S_y)$ consists of two parts: the diagonal part linear in $k_y(k_x)$ and the nondiagonal part quadratic in $k_\pm$. The diagonal part, which relates the wave vector $k_y$ ($k_x$) to $S_x$ ($S_y$), will give the main contribution to CISP.

The velocity operator in the $k$-cubic Rashba model can also be obtained by the projection technique,

$$\tilde{v}_x = \frac{\hbar k_x}{m_h} + \frac{3i\alpha}{\hbar}(k_-^2\sigma_+ - k_+^2\sigma_-), \tag{35}$$

which is consistent with the relation $\tilde{v}_x = \frac{1}{\hbar}\partial H_{k^3}/\partial k_x$.

### B. Impurity vertex correction

Now, we calculate the ESS in the framework of the linear response theory based on the $k$-cubic Rashba model (23). In doing this, we take the vertex correction of impurities into account. The free retarded Green function has the form

$$G_0^R(\mathbf{k},E) = \frac{E - \varepsilon(\mathbf{k}) + \sum_i d_i\sigma_i}{(E - E_+ + i\eta)(E - E_- + i\eta)}, \tag{36}$$

where $\eta$ is an infinitesimal positive number. We assume impurities to be distributed randomly in the form $V_r(\mathbf{r}) = V_0\Sigma_i\delta(\mathbf{r} - \mathbf{R}_i)$, where $V_0$ is the strength. With the Born approximation, the self-energy, diagonal in the spin space, is given by

$$\mathrm{Im}[\Sigma_0^R(\mathbf{k},E)] = \frac{n_i V_0^2\pi}{2}(D_+ + D_-), \tag{37}$$

where $n_i$ is the impurity density, and the density of states for two spin-split branches of the HH1 subband reads

$$D_\pm(k) = \frac{m_h}{2\pi\hbar^2}\left|1 \pm \frac{3m_h\alpha k}{\hbar^2}\right|^{-1}. \tag{38}$$

So the configuration-averaged Green function is given by

$$G^R(\mathbf{k},E) = \frac{E - \varepsilon(k) + i\Gamma_0 + \sum_i d_i\sigma_i}{(E - E_+ + i\Gamma_0)(E - E_- + i\Gamma_0)}, \tag{39}$$

where $\Gamma_0 = -\mathrm{Im}[\Sigma_0^R(\mathbf{k},E)] = \frac{\hbar}{2\tau}$, and $\tau$ is the momentum relaxation time. In the ladder approximation, the Streda–Smrcka formula (15) for the ESS $\chi$ will reduce to

$$\chi_{\alpha\beta} = e\hbar\int\frac{dE}{2\pi}\left(-\frac{\partial f(E)}{\partial E}\right)\int\frac{d^2k}{(2\pi)^2}\mathrm{Tr}[\tilde{S}_\alpha G^R \Upsilon_\beta G^A], \tag{40}$$

where $\tilde{\mathbf{S}}$ is given by Eqs. (29)–(31) and the vertex function $\Upsilon_\beta(\mathbf{k})$ satisfies the self-consistent equation[45]

$$\Upsilon_\beta = \tilde{v}_\beta + n_i V_0^2\int\frac{d^2k}{(2\pi)^2}G^R(\mathbf{k},E)\Upsilon_\beta G^A(\mathbf{k},E). \tag{41}$$

Suppose the electric field is along the $x$ direction, we solve the vertex function $\Upsilon_x$ iteratively and get the first-order correction to $\Upsilon_x$ as

$$\Delta\Upsilon_x^{(1)} = n_i V_0^2 \int \frac{kdkd\theta}{(2\pi)^2} \frac{\begin{pmatrix} E-\varepsilon(\mathbf{k}) & i\alpha k_-^3 \\ -i\alpha k_+^3 & E-\varepsilon(\mathbf{k}) \end{pmatrix} \begin{pmatrix} \frac{\hbar k_x}{m_h} & \frac{3i\alpha}{\hbar}k_-^2 \\ -\frac{3i\alpha}{\hbar}k_+^2 & \frac{\hbar k_x}{m_h} \end{pmatrix} \begin{pmatrix} E-\varepsilon(\mathbf{k}) & i\alpha k_-^3 \\ -i\alpha k_+^3 & E-\varepsilon(\mathbf{k}) \end{pmatrix}}{[(E-E_+)^2+\Gamma_0^2][(E-E_-)^2+\Gamma_0^2]}. \tag{42}$$

Note that $E_\pm$ and $\Gamma_0$ are independent of $\theta$, and all the terms in the numerator of the integrand contain something like $\exp(\pm i\theta)$, etc., so the integral over $\theta$ from 0 to $2\pi$ in Eq. (42) vanishes. Furthermore, the higher-order terms for the vertex correction also vanish, which is quite different from the vertex correction in the linear-**k** Rashba model.[8] The same situation occurs for $\Upsilon_y$. The above results agree with the previous work.[37,53] The calculation of the spin polarization is straightforward, and to the lowest order in Fermi momentum $k_\pm^F$ and $\alpha$, only the term proportional to $S_0$ contributes to the spin polarization. The final result reads

$$\chi_{yx} = -\chi_{xy} = \frac{eS_0\tau m_h E_F}{\hbar^3\pi} = S_0 n_h \frac{e\tau}{\hbar}, \tag{43}$$

$$\chi_{xx} = \chi_{yy} = 0, \tag{44}$$

where $n_h$ is the hole density, $E_F$ is the Fermi energy, and only the leading term in $E_F$ is retained.

In the first-order Born approximation, the longitudinal conductivity of a 2DHG is equal to

$$\sigma_{xx} = \frac{e^2\tau E_F}{\hbar^2\pi}. \tag{45}$$

Thus, by combining expressions (43) and (45), we have the ratio

$$\frac{\langle\tilde{S}_y\rangle}{\langle j_x\rangle} = \frac{\chi_{yx}}{\sigma_{xx}} = \frac{S_0 m_h}{e\hbar} = \frac{\alpha m_0 m_h}{e\hbar^3\gamma_2}. \tag{46}$$

The formula above can also be obtained from the expression of the spin operator (30) and the velocity operator (35) by neglecting the nondiagonal part in the spin operator and the anomalous part in the velocity operator, i.e., $\tilde{S}_y \approx S_0 k_x$ and $j_x \approx e\hbar k_x/m_h$. Obviously, this ratio depends only on the material parameters, but not on the impurity scattering or the carrier density in the low density limit. Meanwhile, since both the current and spin polarization can be experimentally measured, relation (46) may be invoked to experimentally obtain the $k$-cubic Rashba coefficient $\alpha$.

### C. Comparing the current-induced spin polarization of a two-dimensional hole gas and a two-dimensional electron gas

The CISP of a 2DHG manifests several features different from that of 2DEG. To illustrate this, let us first take a look at the CISP of a 2DEG. The electric spin susceptibility is given by $\chi_{yx}=2e\tau\alpha_e m_e/\hbar^2$, where $m_e$ is the effective mass of an electron and $\alpha_e$ is the linear Rashba coefficient. The vertex correction due to the linear Rashba spin splitting is nontrivial.[8,54] With the longitudinal conductivity of 2DEG $\sigma_{xx}=e^2\tau E_F/\hbar^2\pi$, we find that the ratio of spin polarization to the current for the 2DEG is

$$\frac{\langle S_y^{(e)}\rangle}{\langle j_x\rangle} = \frac{\chi_{yx}}{\sigma_{xx}} = \frac{2\pi m_e\alpha_e}{eE_F}. \tag{47}$$

Compared with Eq. (46), we find that the CISP of a 2DEG is inversely proportional to the Fermi energy. This means that the ratio for the 2DEG decreases for heavier doping. This different Fermi-energy dependence stems from the different types of spin orientation for a 2DEG and a 2DHG.

The spin orientation, which is the expectation value of the spin operator **S** for an eigenstate, is given by

$$\langle k\mu|\tilde{S}_x|k\mu\rangle = -S_0 k\sin\theta + \mu k^2 S_1\sin\theta, \tag{48}$$

$$\langle k\mu|\tilde{S}_y|k\mu\rangle = S_0 k\cos\theta - \mu k^2 S_1\cos\theta, \tag{49}$$

$$\langle k\mu|\tilde{S}_z|k\mu\rangle = 0, \tag{50}$$

for a 2DHG, and

$$\langle k\mu|S_x^{(e)}|k\mu\rangle = -\mu\sin\theta, \tag{51}$$

$$\langle k\mu|S_y^{(e)}|k\mu\rangle = \mu\cos\theta, \tag{52}$$

$$\langle k\mu|S_z^{(e)}|k\mu\rangle = 0, \tag{53}$$

for a 2DEG. In the following, we take $\langle\mathbf{S}\rangle_{k\mu}$ as short for the spin orientation above. Equations (51) and (52) show that the spin orientation for a 2DEG depends on the spin index $\mu$, which has opposite values for the two spin-splitting states. However, for a 2DHG, the first term in Eqs. (48) and (49) is independent of the spin index $\mu$. Hence, when $k$ is small, this spin-index-independent term will dominate over the $k^2$ term, leading to the same spin orientation for the hole state with opposite $\mu$. This is quite different from the electron case. The following interesting question may be raised: Why do holes with opposite $\mu$ have the same spin orientation? In the following, we will analyze this problem and try to find the origin of this particular spin orientation for a 2DHG.

Let us first have a look at the electron case. Due to the spin-orbit coupling and inversion asymmetry, the twofold degeneracy of a subband is lifted. For a given $k$, we denote two spin-split states as $|+\rangle = \cos\frac{\theta}{2}e^{-i\phi}|\frac{1}{2}\rangle_z + \sin\frac{\theta}{2}|-\frac{1}{2}\rangle_z$ and $|-\rangle = -\sin\frac{\theta}{2}e^{-i\phi}|\frac{1}{2}\rangle_z + \cos\frac{\theta}{2}|-\frac{1}{2}\rangle_z$, where $|\pm\frac{1}{2}\rangle_z$ are the eigenstates of $\sigma_z$. It is easy to verify that $|+\rangle$ and $|-\rangle$ have opposite spin orientations, namely, $\langle+|\vec{\sigma}|+\rangle = -\langle-|\vec{\sigma}|-\rangle$.

Similar to a 2DEG, two spin-split hole states in the subspace $|\pm\frac{3}{2}\rangle$ can be constructed as $|+\rangle=\cos\frac{\theta}{2}e^{-i\phi}|\frac{3}{2}\rangle+\sin\frac{\theta}{2}|-\frac{3}{2}\rangle$ and $|-\rangle=-\sin\frac{\theta}{2}e^{-i\phi}|\frac{3}{2}\rangle+\cos\frac{\theta}{2}|-\frac{3}{2}\rangle$. By Eqs. (8) and (9), we can verify that the matrix elements of $\hat{S}_x$ and $\hat{S}_y$ between $|\frac{3}{2}\rangle$ and $|-\frac{3}{2}\rangle$ vanish, and $\langle\pm|\hat{S}_x|\pm\rangle=\langle\pm|\hat{S}_y|\pm\rangle=0$. This indicates that in the subspace $|\pm\frac{3}{2}\rangle$, any superposition of $|\pm\frac{3}{2}\rangle$ will not give rise to the spin orientation along the $x$ or $y$ direction. Thus, it is necessary to take the higher order perturbation into account, in particular, the perturbation from coupling between $|\pm\frac{3}{2}\rangle$ and $|\pm\frac{1}{2}\rangle$.

Now we give the outline on the origin of the hole spin orientation by the perturbation procedure (a more systematic method can be found in Appendix A). Suppose the HH1$\pm$ states $\Psi_{hh,\pm}$ can be expanded as

$$\Psi_{hh,\pm}=\Psi^{(0)}_{hh,\pm}+\Psi^{(1)}_{hh,\pm}+\Psi^{(2)}_{hh,\pm}+\cdots, \tag{54}$$

where $\Psi^{(i)}_{hh,\pm}$ denotes the $i$th-order perturbed wave function. With the basis $|n,\lambda_h\rangle$ [Eq. (12)] and the zeroth-order term

$$\Psi^{(0)}_{hh,\pm}=\left|1,\pm\tfrac{3}{2}\right\rangle, \tag{55}$$

we have the first-order correction as

$$\Psi^{(1)}_{hh,+}=\frac{\left|2,\frac{1}{2}\right\rangle\left\langle 2,\frac{1}{2}\right|R^{\dagger}\left|1,\frac{3}{2}\right\rangle}{E_{1,3/2}-E_{2,1/2}}+\frac{\left|1,-\frac{1}{2}\right\rangle\left\langle 1,-\frac{1}{2}\right|T^{\dagger}\left|1,\frac{3}{2}\right\rangle}{E_{1,3/2}-E_{1,-1/2}}+\frac{\left|2,\frac{3}{2}\right\rangle\left\langle 2,\frac{3}{2}\right|V_a\left|1,\frac{3}{2}\right\rangle}{E_{1,3/2}-E_{2,3/2}}, \tag{56}$$

$$\Psi^{(1)}_{hh,-}=\frac{\left|1,\frac{1}{2}\right\rangle\left\langle 1,\frac{1}{2}\right|T\left|1,-\frac{3}{2}\right\rangle}{E_{1,-3/2}-E_{1,1/2}}-\frac{\left|2,-\frac{1}{2}\right\rangle\left\langle 2,-\frac{1}{2}\right|R\left|1,-\frac{3}{2}\right\rangle}{E_{1,-3/2}-E_{2,-1/2}}+\frac{\left|2,-\frac{3}{2}\right\rangle\left\langle 2,-\frac{3}{2}\right|V_a\left|1,-\frac{3}{2}\right\rangle}{E_{1,-3/2}-E_{2,-3/2}}, \tag{57}$$

and the second-order correction reads

$$\Psi^{(2)}_{hh,+}=\frac{\left|1,\frac{1}{2}\right\rangle\left\langle 1,\frac{1}{2}\right|V_a\left|2,\frac{1}{2}\right\rangle\left\langle 2,\frac{1}{2}\right|R^{\dagger}\left|1,\frac{3}{2}\right\rangle}{(E_{1,3/2}-E_{1,1/2})(E_{1,3/2}-E_{2,1/2})}+\frac{\left|1,\frac{1}{2}\right\rangle\left\langle 1,\frac{1}{2}\right|R^{\dagger}\left|2,\frac{3}{2}\right\rangle\left\langle 2,\frac{3}{2}\right|V_a\left|1,\frac{3}{2}\right\rangle}{(E_{1,3/2}-E_{1,1/2})(E_{1,3/2}-E_{2,3/2})}+\cdots, \tag{58}$$

and

$$\Psi^{(2)}_{hh,-}=-\frac{\left|1,-\frac{1}{2}\right\rangle\left\langle 1,-\frac{1}{2}\right|V_a\left|2,-\frac{1}{2}\right\rangle\left\langle 2,-\frac{1}{2}\right|R\left|1,-\frac{3}{2}\right\rangle}{(E_{1,-3/2}-E_{1,-1/2})(E_{1,-3/2}-E_{2,-1/2})}-\frac{\left|1,-\frac{1}{2}\right\rangle\left\langle 1,-\frac{1}{2}\right|R\left|2,-\frac{3}{2}\right\rangle\left\langle 2,-\frac{3}{2}\right|V_a\left|1,-\frac{3}{2}\right\rangle}{(E_{1,-3/2}-E_{1,-1/2})(E_{1,-3/2}-E_{2,-3/2})}+\cdots. \tag{59}$$

Here, $E_{n,\lambda_h}$ stands for the eigenenergy of the state $|n,\lambda_h\rangle$. From Eqs. (8) and (9), we can see that when $n=1$, the only nonvanishing terms are $\langle 1,\frac{3}{2}|\hat{S}_{x(y)}|1,\frac{1}{2}\rangle$ and $\langle 1,-\frac{3}{2}|\hat{S}_{x(y)}|1,-\frac{1}{2}\rangle$. Up to the second-order perturbation, two types of terms can contribute to $\langle\Psi_{hh,\pm}|\hat{S}_{x(y)}|\Psi_{hh,\pm}\rangle$.

The first type stems from the first-order perturbation by the $T$ operator in the Luttinger Hamiltonian [Eq. (3)], which couples $|1,-\frac{1}{2}\rangle$ ($|1,\frac{1}{2}\rangle$) to $|1,-\frac{3}{2}\rangle$ ($|1,\frac{3}{2}\rangle$) [the second term in Eq. (56) or (57)]. So the matrix element $\langle\Psi_{hh,+}|\hat{S}_x|\Psi_{hh,-}\rangle$ is equal to

$$\langle\Psi^{(0)}_{hh,+}|\hat{S}_x|\Psi^{(1)}_{hh,-}\rangle+\langle\Psi^{(1)}_{hh,+}|\hat{S}_x|\Psi^{(0)}_{hh,-}\rangle=\frac{3}{4\pi^2}L_z^2k_-^2. \tag{60}$$

It is obvious that the above formula is just the off-diagonal element in the $\tilde{S}_x$ matrix [Eq. (29)], with the first term in square bracket of $S_1$ [Eq. (33)] retained. This gives the quadratic-$k$ dependence of the spin orientation shown as the second term in Eq. (48).

The second type comes from a joint action of the $R$ in the Luttinger Hamiltonian and the asymmetrical potential $V_a$ [see Eqs. (58) and (59)]. The second-order perturbation contributes to $\langle\Psi_{hh,+}|\hat{S}_x|\Psi_{hh,+}\rangle$ with

$$\langle\Psi^{(0)}_{hh,+}|\hat{S}_x|\Psi^{(2)}_{hh,+}\rangle+\langle\Psi^{(2)}_{hh,+}|\hat{S}_x|\Psi^{(0)}_{hh,+}\rangle+\langle\Psi^{(1)}_{hh,+}|\hat{S}_x|\Psi^{(1)}_{hh,+}\rangle=-\frac{512\gamma_2L_z^4eFm_0k_y}{9\pi^6\hbar^2(3\gamma_1+10\gamma_2)(\gamma_1-2\gamma_2)}. \tag{61}$$

This term is just the diagonal element in Eq. (29), which leads to the first term in Eq. (48) and is responsible for the identical spin orientation for two spin-splitting hole states in the small $k$ regime.

The spin splitting between HH$\pm$ depends on the coupling between $|1,\frac{3}{2}\rangle$ and $|1,-\frac{3}{2}\rangle$ through higher-order perturbation. Different from the electron case, the direct coupling will not cause the $x$-direction or $y$-direction spin orientation. Instead, it results from the coupling between $|1,\frac{3}{2}\rangle$ ($|1,-\frac{3}{2}\rangle$) and $|1,\frac{1}{2}\rangle$ ($|1,-\frac{1}{2}\rangle$). For two LH1 states, denoted as $\Psi_{lh,\pm}$, such coupling will lead to the spin orientations of $\Psi_{lh,+}$ opposite to $\Psi_{hh,+}$, and that of $\Psi_{lh,-}$ opposite to $\Psi_{hh,-}$. Thus, the total spin orientation of the 2DHG is conserved, though $\Psi_{hh,+}$ and $\Psi_{hh,-}$ have the same spin orientation in the low hole density regime.

## IV. NUMERICAL RESULTS FOR CURRENT-INDUCED SPIN POLARIZATION IN A TWO-DIMENSIONAL HOLE GAS

Based on the calculated eigenstates and eigenenergies of the total Hamiltonian (1), in this section, we will work out the spin polarization by using the Bastin version of the Kubo formula (14) in the first-order Born approximation. Of course, the validity of such approximation depends on the vanishing vertex correction as mentioned above.

Our numerical results with an expanded basis set of $N$ basis functions ($N$ is much larger than 8 used in the previous section) show that for a quantum well with infinitely high potential barrier, when increasing $N$, the eigenenergies very quickly converge to the exact solutions formulated by Huang *et al.*[55] For example, for the quantum well with width $L_z=83$ Å, several lowest hole subbands obtained with $N=20$ are almost identical to the exact results. Even for $N=8$, the dispersion of the lowest heavy- and light-hole subbands is in good agreement with the exact results, demonstrating the validity of the truncation procedure in previous section and

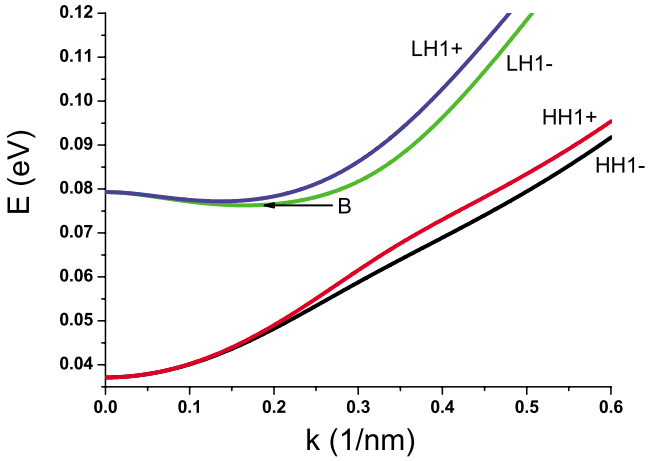


FIG. 1. (Color online) Dispersion relation for a quantum well with infinite barrier in an electric field. HH1± and LH1± denote the two lowest heavy- and light-hole subbands, respectively. The parameters for calculation are the well width $L_z$=83 Å, the field strength $F$=50 kV/cm, $\gamma_1$=7, and $\gamma_2$=1.9.

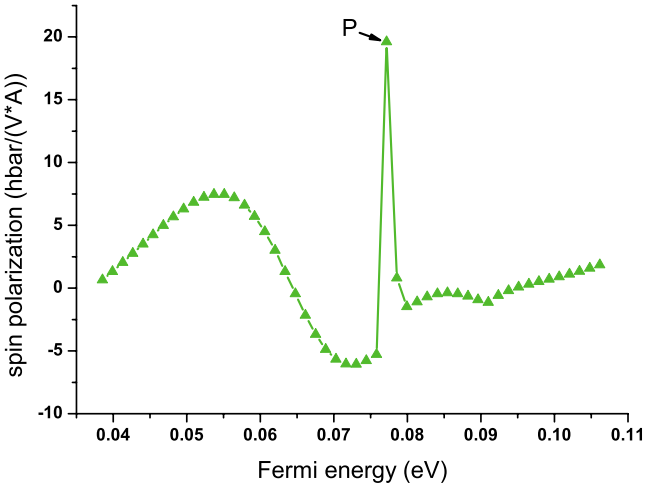


FIG. 2. (Color online) The calculated ESS versus Fermi energy. The scattering induced broadening $\eta$ is taken as $1.65\times10^{-5}$ eV, corresponding to the relaxation time $\tau=2\times10^{-11}$ s. All the other parameters are the same as in Fig. 1. The spin polarization peak marked with P corresponds to the energy minimum of the lowest light-hole subband marked as B in Fig. 1.

Appendix A. Figure 1 plots the dispersion curves and spin splitting of hole subbands in the quantum well in the presence of an electric field. Due to the heavy and light-hole mixture effect, the energy minimum of the lowest light-hole subband, marked by $B$ in the figure, significantly deviates from the $\Gamma$ point.

For the electric spin susceptibility, we calculate $\chi_{yx}$ only, because $\chi_{xx}=\chi_{yy}=0$ and $\chi_{xy}=\chi_{yx}$ as indicated by Eq. (21). After some algebra, we can divide ESS in Eq. (14) into an intrasubband part $\chi_{yx}^{I}$ and an intersubband part $\chi_{yx}^{II}$, which are expressed, respectively, as

$$\chi_{yx}^{I}=\frac{e\hbar}{2\pi}\int\frac{d^2k}{(2\pi)^2}\sum_{\nu}\langle k\nu|\hat{S}_y|k\nu\rangle\langle k\nu|\hat{v}_x|k\nu\rangle\frac{A_\nu^2}{2}, \quad (62)$$

$$\chi_{yx}^{II}=\frac{e\hbar}{2\pi}\int\frac{d^2k}{(2\pi)^2}\sum_{\nu>\nu'}\mathrm{Re}(\langle k\nu|\hat{S}_y|k\nu'\rangle\langle k\nu'|\hat{v}_x|k\nu\rangle)A_\nu A_{\nu'}. \quad (63)$$

Here, Re denotes the real part, and $\nu$ and $\nu'$ stand for the hole subband. In the first-order Born approximation, the spectral function $A_\nu$ can be expressed as

$$A_\nu=\frac{2\eta}{[(E-E_\nu)^2+\eta^2]^2}, \quad (64)$$

where $\eta=\frac{\hbar}{2\tau}$.

A typical curve for the CISP is plotted in Fig. 2. From the calculation, we find that the main contribution to CISP comes from the intrasubband term, which can be understood by Eqs. (62) and (63). In the limit $\eta\to0$, the spectral function $A_\nu$ tends to be the delta function $2\pi\delta(E-E_\nu)$, making the intersubband term $A_\nu A_{\nu'}$ vanish except for an accidental degeneracy. Several features in Fig. 2 are worth pointing out. First, in the low-doping regime where only HH1± states near $\Gamma$ point are occupied, spin polarization exhibits a linear dependence on the Fermi energy. Second, with the hole density increased, the spin polarization increases at first, then decreases after reaching a maximum value, and even changes its sign when the hole density is large enough. Third, when the doping is so heavy that the light-hole subband is occupied, a sharp peak for the spin polarization may be observed, marked as P in Fig. 2.

To understand these features, we turn back to Eq. (62), as the main contribution to the spin polarization stems from this intrasubband term. Based on numerical results as well as Eq. (49), we adopt a function $J_\nu(k)$ to express the amplitude of the spin orientation associated with the subband $\nu$, i.e.,

$$(S_y)_{\nu\nu}=J_\nu(k)\cos\theta.$$

Then, with

$$(v_x)_{\nu\nu}=\frac{1}{\hbar}\frac{\partial E_\nu}{\partial k_x}=\frac{1}{\hbar}\frac{\partial E_\nu(k)}{\partial k}\cos\theta$$

and

$$A_\nu^2=\frac{4\pi\tau}{\hbar}\delta(E_F-E_\nu),$$

we rewrite Eq. (62) as

$$\chi_{yx}=\frac{e\tau}{4\pi\hbar}\sum_{\nu}k_\nu^F J_\nu(k_\nu^F), \quad (65)$$

where $k_\nu^F$ is the Fermi momentum with the hole subband $\nu$.

In the $k$-cubic Rashba model, in which only the lowest heavy-hole subband HH1± is concerned, up to the first-order in $\alpha$, the Fermi momentum can be expressed as $k_\mu^F=\frac{\sqrt{2m_h E_F}}{\hbar}-\mu\frac{2\alpha m_h^2 E_F}{\hbar^4}$. Combined with Eq. (49), we obtain

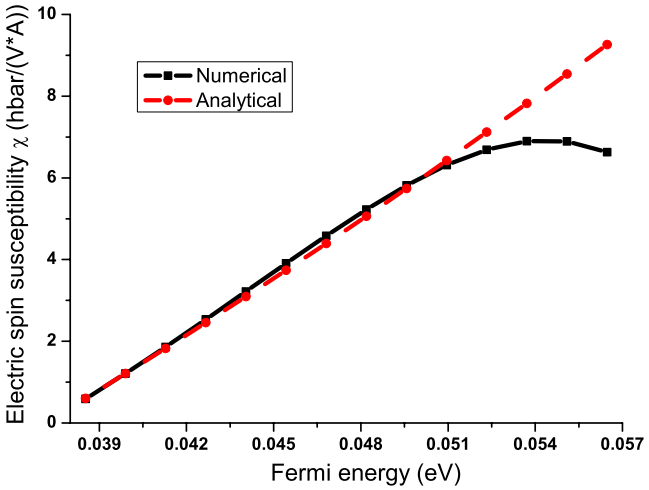


FIG. 3. (Color online) Numerically calculated ESS as function of Fermi energy (black-square line) compared to the analytical results (red-circle line).

$$\chi_{yx} = \frac{e\tau m_h S_0 E_F}{\pi\hbar^3} + \frac{3e\tau m_h^3 \alpha S_1 E_F^2}{\pi\hbar^7}. \tag{66}$$

The first term on the right hand side of Eq. (66), resulting from the spin-independent part, is identical to Eq. (43), while the second term, proportional to $E_F^2$, can be safely ignored in the low density regime. As shown in Fig. 3, the analytical results of the electric spin susceptibility [Eq. (66)] agree well with the numerical ones, demonstrating the applicability of the $k$-cubic Rashba model (23) in the low-doping regime. However, for higher hole density, numerical results show a drop of the $\chi$ due to the heavy- and light-hole mixing effect, which is certainly beyond the simple $k$-cubic Rashba model.

For numerical results, similar to the derivation above, we may divide $J_\nu$ into a spin-dependent part and a spin-independent one, namely, $J_{\nu\mu}=J_\nu^i+\mu J_\nu^d$. Then the ESS can be expressed as

$$\chi_{yx} = \chi_{yx}^i + \chi_{yx}^d, \tag{67}$$

in which the spin-independent and -dependent parts respectively, reads

$$\chi_{yx}^i = \frac{e\tau}{2\pi\hbar}\sum_\nu J_\nu^i \frac{k_{\nu+}^F + k_{\nu-}^F}{2}, \tag{68}$$

$$\chi_{yx}^d = \frac{e\tau}{2\pi\hbar}\sum_\nu J_\nu^d \frac{k_{\nu+}^F - k_{\nu-}^F}{2}. \tag{69}$$

Obviously, $\chi_{yx}^i$ depends on the average of Fermi wave numbers, while $\chi_{yx}^d$ depends on the Fermi wave number difference between two spin-split branches. In most cases, owing to the fact that the spin splitting is small compared to the Fermi energy, $\chi_{yx}^i$ will dominate the spin polarization. In Fig. 4(a), we plot the magnitude of spin orientation associated with the subband HH1±, denoted by $J_{h\pm}$, and the corresponding spin-dependent part $J_h^d$ and spin-independent part $J_h^i$. They are related through $J_h^d=(J_{h+}-J_{h-})/2$ and $J_h^i=(J_{h+}+J_{h-})/2$. Figure 4 indicates that for most values of $k$, $J_h^d$ is larger than $J_h^i$. Compared to the intrasubband contribution in Fig. 2, the spin-independent magnitude of the spin polarization $J_h^i$ [green dotted line in Fig. 4(a)] has a similar behavior: first, linearly increasing with $k$, then decreasing with $k$ increased, and even changing the sign for larger $k$.

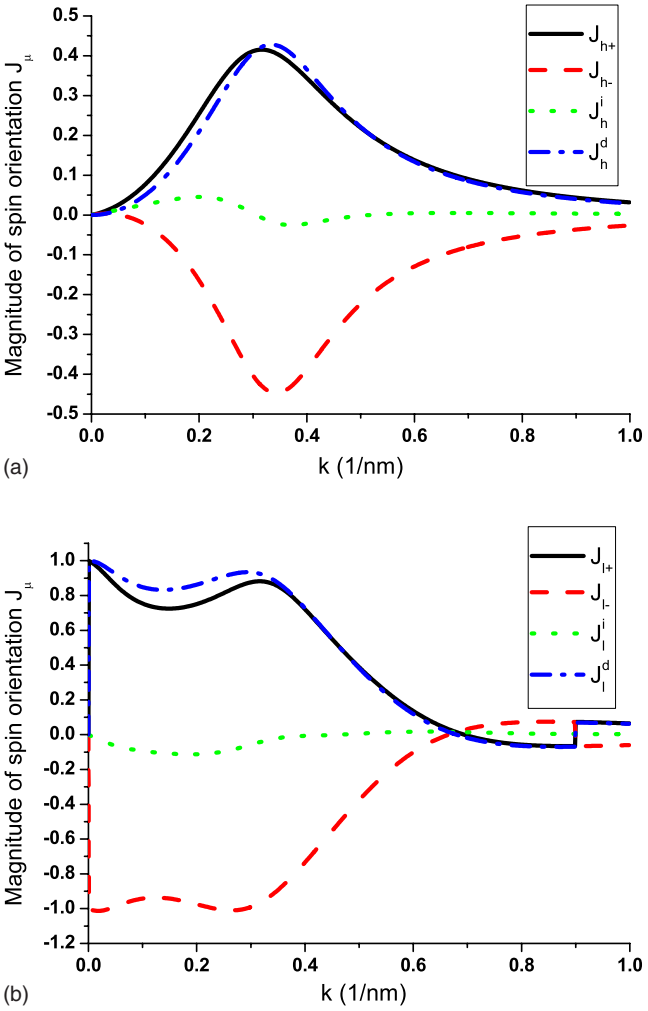


FIG. 4. (Color online) The magnitude of the spin orientation for (a) the lowest heavy hole subband and (b) the lowest light-hole subband. In (a), the black solid line and red dashed line represent $J_{h+}$ and $J_{h-}$, respectively, while the green dotted line and blue dashed dotted line denote the spin-independent part $J_h^i$ and spin-dependent part $J_h^d$, respectively. The same notions are also applied to (b).

A pronounced peak of CISP may appear when the Fermi energy just crosses the bottom of the lowest light-hole subband LH1−. As amplified in Fig. 5, in the dispersion relation of the subband LH1±, the wave numbers $k_{l\pm}^0$ corresponding to the energy minimum $E_{l\pm}^0$ significantly deviate from the $k=0$ point. Around the energy minimum, the energy dispersion can be approximated as $E_{l\mu}(k)=E_{l\mu}^0+\frac{1}{2}\frac{\partial^2 E_{l\mu}(k)}{\partial k^2}(k-k_{l\mu}^0)^2$. Assuming the above energy dispersion and a constant magnitude of $J_{l\mu}$, we obtain

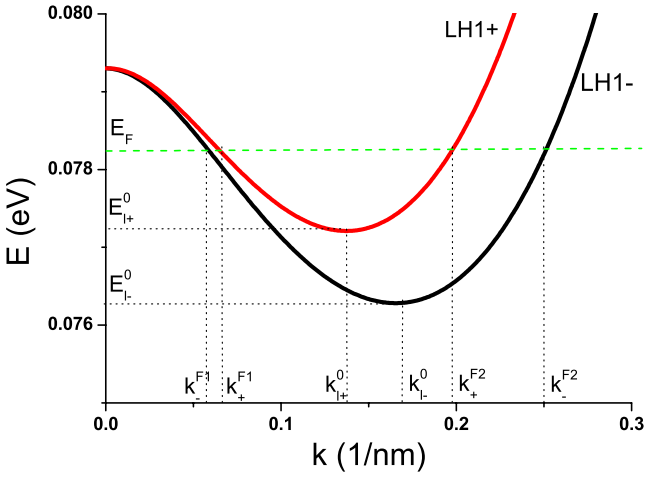


FIG. 5. (Color online) Dispersion relation of the lowest light-hole subband LH1±.

$$\chi_{yx}^{\mu} = \frac{e\tau}{2\pi\hbar} k_{l\mu}^{0} J_{l\mu}(k_{l\mu}^{0}), \tag{70}$$

where $k_{l\mu}^{0} \simeq (k_{\mu}^{F1} + k_{\mu}^{F2})/2$, and $k_{\pm}^{F1}$ and $k_{\pm}^{F2}$, respectively, denote two different Fermi wave numbers for LH1± (Fig. 5). By Eq. (70) and Fig. 4(b), we can see since $J_{l+}$ and $J_{l-}$ are large in the absolute value but almost opposite in sign, when $E_{l+}^{0} > E_F > E_{l-}^{0}$, a large spin polarization $e\tau k_{l-}^{0} J_{l-}/2\pi\hbar$ is expected; on the other hand, when $E_F > E_{l+}^{0} > E_{l-}^{0}$, the contributions of LH1± to the spin polarization cancel each other to some extent, resulting in

$$\chi_{yx} = \frac{e\tau}{2\pi\hbar}[(k_{l-}^{0} + k_{l+}^{0}) J_l^{i} + (k_{l+}^{0} - k_{l-}^{0}) J_l^{d}]. \tag{71}$$

As $J_l^{i}$ is much smaller than $J_l^{d}$ or $J_{l\pm}$, and $k_{l+}^{0} \approx k_{l-}^{0}$, both terms in Eq. (71) are small compared to the case when only LH_ is occupied. Apparently, the peak width depends on the spin splitting between LH_ and LH$_+$.

The temperature dependence of the peak is plotted in Fig. 6. Near the polarization peak, if we only take into account LH1±, ESS is expressed by

$$\chi_{yx} = \frac{e\tau}{2\pi\hbar} \sum_{\mu} f(E_{l\mu}^{0}) k_{l\mu}^{0} J_{l\mu}(k_{l\mu}^{0}). \tag{72}$$

At zero temperature, the Fermi distribution function $f(E)$ becomes the step function $\theta(E_f - E)$, which reproduces the above analysis. At finite temperature $T$, if we approximate $k_{l\mu}^{0} J_{l\mu}(k_{l\mu}^{0}) \simeq \mu k_l^{0} J_l$, and expand the Fermi distribution function at large $k_B T$ as $f(E) = \frac{1}{2}(1 - \frac{E - E_F}{2k_B T})$ ($k_B$ is Boltzmann constant), then Eq. (72) reduces to

$$\chi_{yx} = \frac{e\tau k_l^{0} J_l}{2\pi\hbar} \frac{E_{l+}^{0} - E_{l-}^{0}}{4k_B T}. \tag{73}$$

So ESS is proportional to the ratio of the spin splitting of the LH1 subband, $E_{l+}^{0} - E_{l-}^{0}$, to thermal energy $k_B T$. When $k_B T$ is much larger than the spin splitting, this pronounced spin polarization peak will smear out.

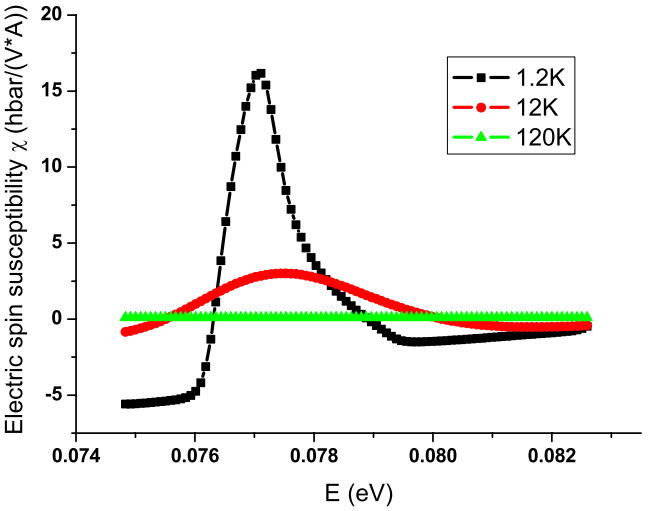


FIG. 6. (Color online) The spin polarization peak at three different temperatures: 1.2, 12, and 120 K.

Now let us estimate the magnitude of the averaged CISP. In the $k$-cubic Rashba model with an applied field $F = 50$ kV/cm, Eq. (32) gives $S_0 = 2.74$ Å for $L_z = 83$ Å and $S_0 = 5.77$ Å for $L_z = 100$ Å. If the typical relaxation time $\tau$ is taken to be $2 \times 10^{-11}$ s and an in-plane electric field strength $E_0 = 10$ V/cm, the Fermi sphere will be shifted by $\Delta k = eE_0\tau/\hbar = 3 \times 10^{-3}$ Å$^{-1}$. By substituting the above data into Eq. (43), we obtain $\langle S_y \rangle / n_h = 0.831\%$ for $L_z = 83$ Å, and $\langle S_y \rangle / n_h = 1.75\%$ for $L_z = 100$ Å. Since $S_0$ is proportional to $L_z^4$, the spin polarization is very sensitive to the thickness of the quantum well. Hence, it is preferable to experimentally detect the CISP in a thicker quantum well. The above estimation gives the same order of magnitude for the spin polarization observed in the experiment of Silov *et al.*[12] In Fig. 7, we plot the averaged spin polarization $\langle S_y \rangle / n_h$ as function of the Fermi energy and of the field $F$ in the inset. The CISP is saturated at about 2% when the field is enhanced.

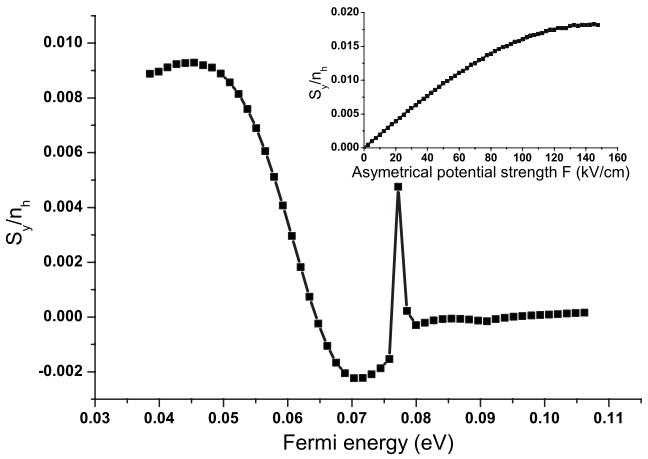


FIG. 7. $\frac{\langle S_y \rangle}{n_h}$ as function of the Fermi energy. Inset: $\frac{\langle S_y \rangle}{n_h}$ as function of applied field strength $F$.

## V. SUMMARY

In conclusion, we have systematically investigated the current induced spin polarization of a 2DHG in the frame of the linear response theory. We introduced the physical quantity of the electric spin susceptibility $\chi$ to describe CISP and give its analytical expression in the simplified $k$-cubic Rashba model. Different from the 2DEG, the CISP of a 2DHG depends linearly on the Fermi energy. The difference in CISP between a 2DHG and a 2DEG results from the different spin orientations in the subband of carriers. We propose that the $k$-cubic Rashba coefficient of a 2DHG can be deduced from the ratio of spin polarization to the current, which is independent of the impurities or disorder effect up to the lowest order. We have also carried out numerical calculations for the CISP. The numerical results are consistent with the analytical one in the low-doping regime, which demonstrates the applicability of the $k$-cubic Rashba model. With the increase in Fermi energy, numerical results show that the spin polarization may be suppressed and even changes its sign. We predict and explain a pronounced spin polarization peak when the Fermi energy crosses over the subband bottom of the LH_. We also discuss the possibility of measuring this spin polarization peak.

## ACKNOWLEDGMENTS

This work was supported by the Research Grant Council of Hong Kong under Grant No. HKU 7041/07P, by the NSF of China (Grants Nos. 10774086 and 10574076), and by the Program of Basic Research Development of China (Grant No. 2006CB921500).

## APPENDIX A: DERIVATION OF THE $k$-CUBIC RASHBA HAMILTONIAN

In this appendix, we present the detailed derivation of the $k$-cubic Rashba model by means of the perturbation method.[40–42,48–52] First, we truncate the Hilbert space of the basis wave functions (12) into the subspace with only the lowest eight states $\mathcal{G}_0=\{|n,\lambda_h\rangle, n=1,2; \lambda_h=\pm\frac{3}{2},\pm\frac{1}{2}\}$. As described in Sec. II, by comparing the lowest HH and LH subband dispersions to the exact solution, the accuracy of such a truncation procedure has been verified. The truncated subspace $\mathcal{G}_0$ can be further cast into two subgroups, $\mathcal{G}_1$ and $\mathcal{G}_2$. $\mathcal{G}_1$ contains two lowest heavy-hole states $\{|1,3/2\rangle,|1,-3/2\rangle\}$, while $\mathcal{G}_2$ keeps the other six states, $\{|1,1/2\rangle,|1,-1/2\rangle,|2,3/2\rangle,|2,-3/2\rangle,|2,1/2\rangle,|2,-1/2\rangle\}$. In this case, the Hamiltonian in the subspace $\mathcal{G}_0$ can be written in the form of block matrices as

$$H_{8\times 8}=\begin{pmatrix}\tilde{H}_{2\times 2} & \tilde{H}_{2\times 6}\\ \tilde{H}_{6\times 2} & \tilde{H}_{6\times 6}\end{pmatrix}, \tag{A1}$$

where

$$\tilde{H}_{2\times 2}=\begin{pmatrix}P(1) & 0\\ 0 & P(1)\end{pmatrix}, \tag{A2}$$

$$\tilde{H}_{6\times 2}=\tilde{H}_{2\times 6}^{\dagger}=\begin{pmatrix}0 & T\\ T^{\dagger} & 0\\ eFG(2,1) & 0\\ 0 & eFG(2,1)\\ R(2,1)k_{+} & 0\\ 0 & -R(2,1)k_{-}\end{pmatrix}, \tag{A3}$$

and

$$\tilde{H}_{6\times 6}=\begin{pmatrix}Q(1) & 0 & R(1,2)k_{+} & 0 & eFG(1,2) & 0\\ 0 & Q(1) & 0 & -R(1,2)k_{-} & 0 & eFG(1,2)\\ R(2,1)k_{-} & 0 & P(2) & 0 & 0 & T\\ 0 & -R(2,1)k_{+} & 0 & P(2) & T^{\dagger} & 0\\ eFG(2,1) & 0 & 0 & T & Q(2) & 0\\ 0 & eFG(2,1) & T^{\dagger} & 0 & 0 & Q(2)\end{pmatrix}. \tag{A4}$$

Here, $P(n)$, $Q(n)$, $G(n,m)$, and $R(n,m)$ are given by

$$P(n)=\frac{\hbar^2}{2m_0}\left[(\gamma_1+\gamma_2)k^2+(\gamma_1-2\gamma_2)\left(\frac{n\pi}{L_z}\right)^2\right], \tag{A5}$$

$$Q(n)=\frac{\hbar^2}{2m_0}\left[(\gamma_1-\gamma_2)k^2+(\gamma_1+2\gamma_2)\left(\frac{n\pi}{L_z}\right)^2\right], \tag{A6}$$

$$G(n,m)=\frac{4L_z nm[(-1)^{n+m}-1]}{\pi^2(m^2-n^2)^2}, \tag{A7}$$

$$R(n,m)=-2\sqrt{3}\frac{\hbar^2\gamma_3}{2m_0}\frac{2inm[(-1)^{n+m}-1]}{L_z(n^2-m^2)}. \tag{A8}$$

Our aim is to perform a transformation which decouples the groups $\mathcal{G}_1$ from $\mathcal{G}_2$, i.e., to make the off-diagonal part $\tilde{H}_{2\times 6}$ and $\tilde{H}_{6\times 2}$ vanish up to the first-order in $k$ and $F$. We divide the total Hamiltonian (A1) into three parts

$$H_{8\times 8}=H_0+H_1+H_2. \tag{A9}$$

The first term $H_0$ is the diagonal matrix elements of $H_{8\times8}$, given by

$$H_0 = \begin{pmatrix} \tilde{H}^{(0)}_{2\times2} & 0 \\ 0 & \tilde{H}^{(0)}_{6\times6} \end{pmatrix}, \tag{A10}$$

with $\tilde{H}^{(0)}_{2\times2}=\mathrm{Diag}[P(1),P(1)]$ and $\tilde{H}^{(0)}_{6\times6}=\mathrm{Diag}[Q(1),Q(1),P(2),P(2),Q(2),Q(2)]$.

The second term $H_1$ is given by

$$H_1 = \begin{pmatrix} 0 & 0 \\ 0 & \tilde{H}^{(1)}_{6\times6} \end{pmatrix}, \tag{A11}$$

where $\tilde{H}^{(1)}_{6\times6}=\tilde{H}_{6\times6}-\tilde{H}^{(0)}_{6\times6}$. The third term $H_2$ contains the nondiagonal part $\tilde{H}_{2\times6}$ and $\tilde{H}_{6\times2}$

$$H_2 = \begin{pmatrix} 0 & \tilde{H}_{2\times6} \\ \tilde{H}_{6\times2} & 0 \end{pmatrix}. \tag{A12}$$

There are three types of perturbation terms in $H_1$ and $H_2$: (1) The $k$-linear $R$ term couples the state $|n,\frac{3}{2}\rangle$ ($|n,-\frac{3}{2}\rangle$) with $|m,\frac{1}{2}\rangle$ ($|m,-\frac{1}{2}\rangle$), where $n$ and $m$ must be of opposite parities due to the presence of $k_z=-i\partial_z$. (2) The $k$-quadratic $T$ term couples $|n,\frac{3}{2}\rangle$ ($|n,-\frac{3}{2}\rangle$) with $|n,-\frac{1}{2}\rangle$ ($|n,\frac{1}{2}\rangle$). (3) The asymmetric potential $V_a$ couples the states with the same spin index and different parities.

The perturbation procedure is as follows. First, $H_2$ will be eliminated by the canonical transformation as

$$H^{(1)}_{8\times8} = \exp[-U^{(1)}]H_{8\times8}\exp[U^{(1)}] = H_{8\times8} + [H_{8\times8},U^{(1)}] + \frac{1}{2}[[H_{8\times8},U^{(1)}],U^{(1)}] + \cdots, \tag{A13}$$

in which $U^{(1)}$ is chosen such that

$$H_2 + [H_0,U^{(1)}] = 0,$$

and the matrix elements read

$$U^{(1)}_{\alpha\beta} = -\frac{(H_2)_{\alpha\beta}}{E_\alpha - E_\beta}, \quad \alpha \neq \beta, \tag{A14}$$

where $E_\alpha$ denotes the energy of the band $\alpha$ at the $\Gamma$ point ($k=0$). After the canonical transformation, the new Hamiltonian is given by

$$H^{(1)}_{8\times8} = H_0 + H_1 + \frac{1}{2}[H_2,U^{(1)}] + [H_1,U^{(1)}] + \frac{1}{2}[[H_1,U^{(1)}],U^{(1)}] + \cdots. \tag{A15}$$

The $H_0$, $H_1$, $\frac{1}{2}[H_2,U^{(1)}]$, and $\frac{1}{2}[[H_1,U^{(1)}],U^{(1)}]$ have the block-diagonal form, while $[H_1,U^{(1)}]$ is non-block-diagonal and contains additional terms first order in $k$. So we divide $H^{(1)}_{8\times8}$ into three parts again

$$H^{(1)}_{8\times8} = H_0 + H^{(1)}_1 + H^{(1)}_2, \tag{A16}$$

in which $H^{(1)}_1=H_1+\frac{1}{2}[H_2,U^{(1)}]+\frac{1}{2}[[H_1,U^{(1)}],U^{(1)}]$, and $H^{(1)}_2=[H_1,U^{(1)}]$. We perform the second canonical transformation $U^{(2)}$, given by

$$U^{(2)}_{\alpha\beta} = -\frac{(H^{(1)}_2)_{\alpha\beta}}{E_\alpha - E_\beta}, \quad \alpha \neq \beta. \tag{A17}$$

This makes the nondiagonal block matrix $H^{(1)}_2$ zero, leading to the Hamiltonian

$$H^{(2)}_{8\times8} = H_0 + H^{(1)}_1 + \frac{1}{2}[H^{(1)}_2,U^{(1)}] + [H^{(1)}_1,U^{(1)}] + \frac{1}{2}[[H^{(1)}_1,U^{(1)}],U^{(1)}] + \cdots. \tag{A18}$$

Now the non-block-diagonal terms of $H^{(2)}_{8\times8}$ vanish up to the desired order in $k$ and $F$. Finally, by mapping the Hamiltonian $H^{(2)}_{8\times8}$ into the lowest heavy-hole subbands, we obtain the $k$-cubic Rashba Hamiltonian Eq. (23).

To obtain the corresponding spin operators in the lowest heavy-hole basis, we should apply the same canonical transformations $U^{(1)}$ and $U^{(2)}$ to the spin operators $S_i$ ($i=x,y,z$). In the eight-state subspace $\mathcal{G}_0$, we find that the spin operator has the block-diagonal form $S_i=\mathrm{Diag}[S^{(1)}_i,S^{(1)}_i](i=x,y,z)$, because there are no matrix elements between the states with different confinement quantum number $n$. Therefore, $S^{(1)}_i$ is a $4\times4$ matrix, given respectively by

$$S^{(1)}_x = \frac{1}{2}\begin{pmatrix} 0 & 0 & \sqrt{3} & 0 \\ 0 & 0 & 0 & \sqrt{3} \\ \sqrt{3} & 0 & 0 & 2 \\ 0 & \sqrt{3} & 2 & 0 \end{pmatrix}, \tag{A19}$$

$$S^{(1)}_y = \frac{i}{2}\begin{pmatrix} 0 & 0 & -\sqrt{3} & 0 \\ 0 & 0 & 0 & \sqrt{3} \\ \sqrt{3} & 0 & 0 & -2 \\ 0 & -\sqrt{3} & 2 & 0 \end{pmatrix}, \tag{A20}$$

$$S^{(1)}_z = \frac{1}{2}\begin{pmatrix} 3 & 0 & 0 & 0 \\ 0 & -3 & 0 & 0 \\ 0 & 0 & 1 & 0 \\ 0 & 0 & 0 & -1 \end{pmatrix}. \tag{A21}$$

Then we apply the transformations $U^{(1)}$ and $U^{(2)}$ to the spin operators, obtaining the new spin operators $\tilde{S}_i=S_i+[S_i,U^{(1)}]+[S_i,U^{(2)}]$ as presented in Eqs. (29)–(31).

## APPENDIX B: HOLE RASHBA TERM

The hole Rashba term has recently attracted the attention of many researchers.[36,41,56] The hole Rashba term breaks the inversion symmetry[40,42] and is expressed as

$$\hat{H}_R = \lambda \begin{pmatrix} 0 & \frac{i\sqrt{3}}{2}k_- & 0 & 0 \\ -\frac{i\sqrt{3}}{2}k_+ & 0 & ik_- & 0 \\ 0 & -ik_+ & 0 & \frac{i\sqrt{3}}{2}k_- \\ 0 & 0 & -\frac{i\sqrt{3}}{2}k_+ & 0 \end{pmatrix}, \quad \text{(B1)}$$

where $\lambda = r_{41}^{8v8v}F$, $r_{41}^{8v8v}$ is a parameter as already given by Winkler for several materials[40] and $F$ is the field strength. If we neglect other asymmetrical potentials and only consider the Rashba term, then the total Hamiltonian is $\hat{H} = H_L + V_c + H_R$. By applying the same perturbation procedure as in Appendix A, we find that both the Hamiltonian and the spin operator have a structure identical to the asymmetrical potential case, as well as the same effective mass $m_h$, $S_1$, and Eq. (34), except for the Rashba coefficient given by

$$\alpha = \frac{3\lambda L_z^2}{4\pi^2} \quad \text{(B2)}$$

and the spin operator parameter

$$S_0 = \frac{3\lambda m_0 L_z^2}{4\pi^2\hbar^2\gamma_2}. \quad \text{(B3)}$$

Here, the hole Rashba coefficient $\alpha$ is proportional to $L_z^2$, while for the asymmetrical potential case, it depends on $L_z^4$. So in most realistic quantum wells, the contribution from the asymmetrical potential plays a more important role than the hole Rashba term, at least 1 or 2 orders of magnitude larger. The physical reason for this may be understood from the origin of the hole Rashba term. The more general form of the Hamiltonian should be $\hat{H} = \hat{H}_{\mathbf{k}\cdot\mathbf{p}} + V_c + eFz$, where the multiband $\mathbf{k}\cdot\mathbf{p}$ Hamiltonian $\hat{H}_{\mathbf{k}\cdot\mathbf{p}}$ includes not only the heavy- and light-hole bands, but also the conduction band, spin split-off band, and remote bands. When we project the Hamiltonian into the subspace of the heavy- and light-hole bands, the combined effects of the $eFz$ and $\mathbf{k}\cdot\mathbf{p}$ mediated by other bands lead to the hole Rashba term, which has a much smaller influence than that directly coupled by the asymmetrical potential. Therefore, hole Rashba term is neglected in this paper for simplicity.


[1] I. Zutic, J. Fabian, and S. Das Sarma, Rev. Mod. Phys. **76**, 323 (2004).
[2] S. A. Wolf, D. D. Awschalom, R. A. Buhrman, J. M. Daughton, S. von Molna, M. L. Roukes, A. Y. Chtchelkanova, and D. M. Treger, Science **294**, 1488 (2001).
[3] D. D. Awschalom and M. E. Flatte, Nat. Phys. **3**, 153 (2007).
[4] M. I. Dyakonov and V. I. Perel, Phys. Lett. **35A**, 459 (1971).
[5] V. M. Edelstein, Solid State Commun. **73**, 233 (1990).
[6] A. G. Aronov, Yu. B. Lyanda-Geller, and G. E. Pikus, Sov. Phys. JETP **73**, 537 (1991).
[7] A. V. Chaplik, M. V. Entin, and L. I. Magarill, Physica E (Amsterdam) **13**, 744 (2002).
[8] J. I. Inoue, G. E. W. Bauer, and L. W. Molenkamp, Phys. Rev. B **67**, 033104 (2003).
[9] O. Bleibaum, Phys. Rev. B **73**, 035322 (2006).
[10] O. Bleibaum, Phys. Rev. B **72**, 075366 (2005).
[11] Y. J. Bao and S. Q. Shen, Phys. Rev. B **76**, 045313 (2007).
[12] A. Yu. Silov, P. A. Blajnov, J. H. Wolter, R. Hey, K. H. Ploog, and N. S. Averkiev, Appl. Phys. Lett. **85**, 5929 (2004).
[13] Y. Kato, R. C. Myers, A. C. Gossard, and D. D. Awschalom, Nature (London) **427**, 50 (2004).
[14] Y. K. Kato, R. C. Myers, A. C. Gossard, and D. D. Awschalom, Phys. Rev. Lett. **93**, 176601 (2004).
[15] V. Sih, R. C. Myers, Y. K. Kato, W. H. Lau, A. C. Gossard, and D. D. Awscholom, Nat. Phys. **1**, 31 (2005).
[16] N. P. Stern, S. Ghosh, G. Xiang, M. Zhu, N. Samarth, and D. D. Awschalom, Phys. Rev. Lett. **97**, 126603 (2006).
[17] C. L. Yang, H. T. He, L. Ding, L. J. Cui, Y. P. Zeng, J. N. Wang, and W. K. Ge, Phys. Rev. Lett. **96**, 186605 (2006).
[18] S. D. Ganichev, S. N. Danilov, P. Schneider, V. V. Belkov, L. E. Golub, W. Wegscheider, D. Weiss, and W. Prettl, J. Magn. Magn. Mater. **300**, 127 (2006).
[19] S. D. Ganichev and W. Prettl, J. Phys.: Condens. Matter **15**, 935 (2003), and references therein.
[20] X. D. Cui, S. Q. Shen, J. Li, Y Ji, W. K. Ge, and F. C. Zhang, Appl. Phys. Lett. **90**, 242115 (2007).
[21] M. G. Vavilov, Phys. Rev. B **72**, 195327 (2005).
[22] S. A. Tarasenko, Phys. Rev. B **73**, 115317 (2006).
[23] M. Trushin and J. Schliemann, Phys. Rev. B **75**, 155323 (2007).
[24] Z. A. Huang and L. B. Hu, Phys. Rev. B **73**, 113312 (2006).
[25] X. H. Ma, L. B. Hu, R. B. Tao, and S. Q. Shen, Phys. Rev. B **70**, 195343 (2004).
[26] L. B. Hu, J. Gao, and S. Q. Shen, Phys. Rev. B **70**, 235323 (2004).
[27] B. Kaestner, Dissertation, University of Cambridge, 2003.
[28] B. Kaestner, Ph.D. thesis, University of Cambridge, 2003.
[29] A. Yu. Silov, J. E. M. Haverkort, N. S. Averkiev, P. M. Koenraad, and J. H. Wolter, Phys. Rev. B **50**, 4509 (1994).
[30] M. Q. Weng, M. W. Wu, and L. Jiang, Phys. Rev. B **69**, 245320 (2004).
[31] Hans-Andreas Engel, Emmanuel I. Rashba, and Bertrand I. Halperin, Phys. Rev. Lett. **98**, 036602 (2007).
[32] M. Milletari, R. Raimondi, and P. Schwab, arXiv:0801.1786 (unpublished).
[33] J. M. Luttinger and W. Kohn, Phys. Rev. **97**, 869 (1955); J. M. Luttinger, *ibid.* **102**, 1030 (1956).
[34] G. Y. Guo, Yugui Yao, and Qian Niu, Phys. Rev. Lett. **94**, 226601 (2005).
[35] B. A. Bernevig, T. L. Hughes, and S. C. Zhang, Phys. Rev. Lett. **95**, 066601 (2005).

[36] B. A. Bernevig and S. C. Zhang, Phys. Rev. Lett. **95**, 016801 (2005).
[37] J. Schliemann and D. Loss, Phys. Rev. B **71**, 085308 (2005).
[38] J. Sinova, S. Murakami, S. Q. Shen, and M. S. Choi, Solid State Commun. **138**, 214 (2006).
[39] E. I. Rashba and E. Ya. Sherman, Phys. Lett. A **129**, 175 (1988).
[40] R. Winkler, *Spin-Orbit Coupling Effects in Two-Dimensional Electron and Hole Systems* (Springer-Verlag, Berlin, 2003).
[41] R. Winkler, Phys. Rev. B **62**, 4245 (2000).
[42] B. F. Zhu and Y. C. Chang, Phys. Rev. B **50**, 11932 (1994).
[43] R. Winkler, Phys. Rev. B **71**, 113307 (2005).
[44] R. Winkler, Phys. Rev. B **70**, 125301 (2004).
[45] G. D. Mahan, *Many-Particle Physics* (Kluwer Academic, New York, 2000).
[46] P. Streda, J. Phys. C **15**, L717 (1982); L. Smrcka and P. Streda, *ibid.* **10**, 2153 (1977).
[47] N. A. Sinitsyn, J. E. Hill, Hongki Min, Jairo Sinova, and A. H. MacDonald, Phys. Rev. Lett. **97**, 106804 (2006).
[48] S. Q. Shen and Z. D. Wang, Phys. Rev. B **61**, 9532 (2000).
[49] B. A. Foreman, Phys. Rev. Lett. **84**, 2505 (2000).
[50] B. A. Foreman, Phys. Rev. B **72**, 165344 (2005).
[51] B. A. Foreman, Phys. Rev. B **72**, 165345 (2005).
[52] B. Habib, E. Tutuc, S. Melinte, M. Shayegan, D. Wasserman, S. A. Lyon, and R. Winkler, Phys. Rev. B **69**, 113311 (2004).
[53] S. Murakami, Phys. Rev. B **69**, 241202(R) (2004).
[54] R. Raimondi, M. Leadbeater, P. Schwab, E. Caroti, and C. Castellani, Phys. Rev. B **64**, 235110 (2001).
[55] K. Huang, J. B. Xia, B. F. Zhu, and H. Tang, J. Lumin. **40-41**, 88 (1988).
[56] M. M. Hasegawa and E. A. de Andrada e Silva, Phys. Rev. B **68**, 205309 (2003).